Three-Dimensional Polymer Structures

DOI: 10.1002/anie.201102518

Fabrication of Arbitrary Three-Dimensional Polymer Structures by Rational Control of the Spacing between Nanobrushes**

*Xuechang Zhou, Xiaolong Wang, Youde Shen, Zhuang Xie, and Zijian Zheng**

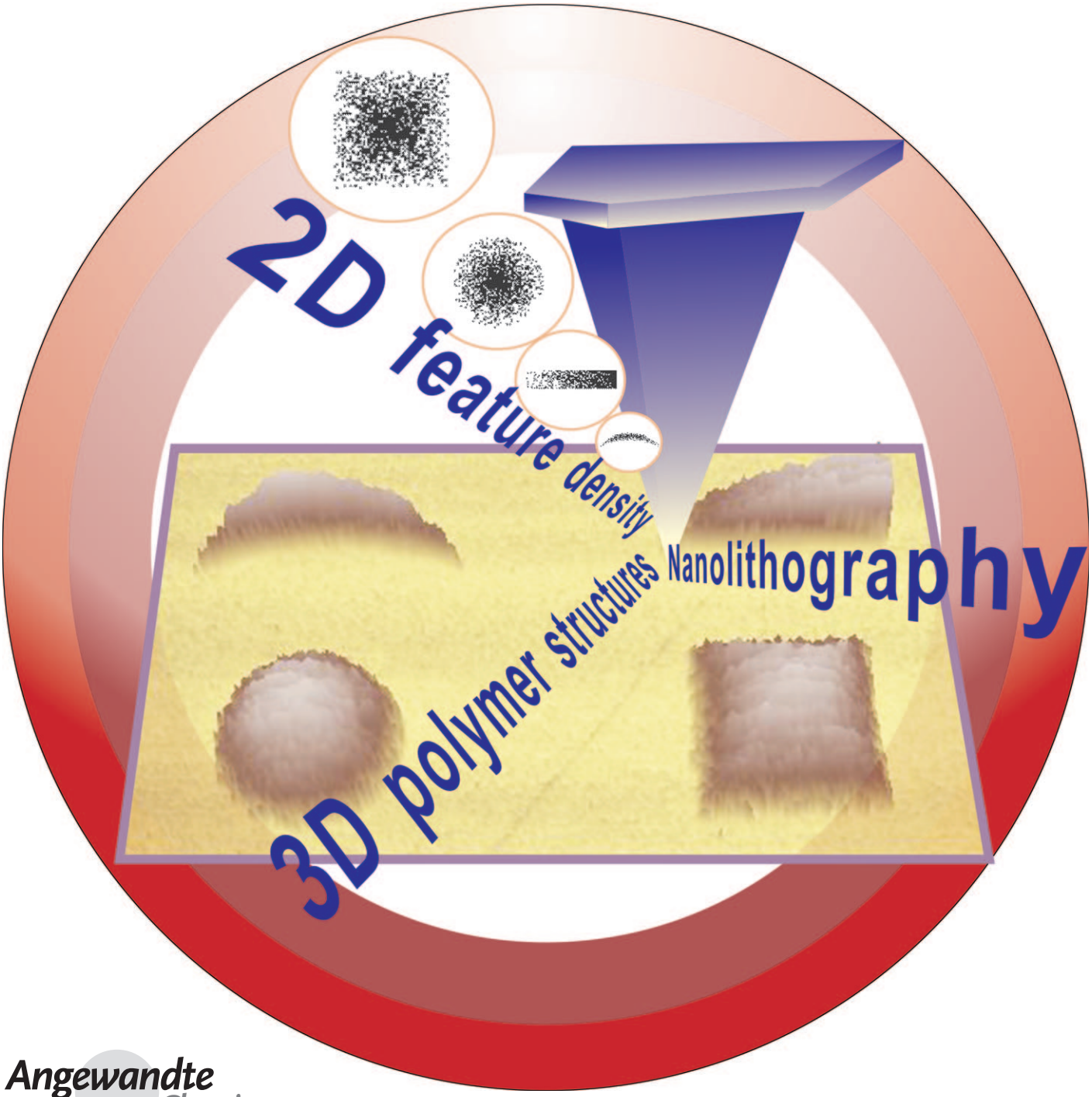

The fabrication of arbitrary three-dimensional (3D) polymer nanostructures with well-defined composition, properties, and morphology is a crucial step towards understanding their fundamental behavior as well as realizing their application in chemistry, biology, and medical science.[1–8] Compared with two-dimensional polymer nanoarrays, which can be routinely fabricated by many nanotechnologies, fabrication of arbitrary 3D polymer structures is much more challenging and remarkably complex because of the simultaneous alignment of in-plane lateral spacings and out-of-plane heights. In the last few years, 3D nanopatterns of polymers have been obtained by scanning probe nanomachining which relies on multiple cycles of serial top-down etching steps of organic resists.[9–11] Although such top-down methods provide highly-resolved topological structures, these methods are limited in the choice of resist materials and tuning the composition and properties of the surfaces is difficult. A more promising strategy is to construct 3D chemically functioning polymer brushes, that is, polymer chains tethered with one end on the surface, by combination of top-down nanofabrication of surface-immobilized initiators and bottom-up surface-initiated polymerization.[12] The principle of morphology control is that polymer brushes of similar chain length, grown from areas of low-grafting density of initiators, form collapsed structures, whereas chains grown from areas of high-grafting density form strechted structures because of the competition between interface energy and chain entropy. As proof-of-concept, arbitrary 3D functional polymer brushes were obtained at nanoscale when nanolithographic tools such as electron-beam (e-beam) lithography[13–18] and dip-pen nanodisplacement lithography (DNL)[19] were used to locally program the grafting density of surface initiators. Nevertheless, precise control and characterization of the grafting density of initiators are still daunting tasks. Furthermore, the throughput for engineering the grafting density is very low, which to a certain extent hampers the application of this method.

Herein, we introduce a novel concept for fabricating arbitrary 3D polymer structures based on the rational design of lateral spacings between arrays of nanosized polymer brushes (nanobrushes). The nanobrushes serve as basic building blocks, of which the morphology evolves from collapsed to stretched structures upon changing of the lateral spacing to their neighboring nanobrushes (Figure 1 a). Therefore, arbitrary 3D topographies are the result of many nanobrushes in different configurations caused by synergistic effects. Previously, several other research groups and we have reported the fabrication of nanobrushes and found that the shape of the nanobrushes is strongly related to their feature size.[13,16,19–21] However, these studies only focused on well-separated nanobrushes. To the best of our knowledge, this is the first article reporting interactions between nanobrushes that are closely positioned. Our spacing-control (or feature-density) method is much more efficient, straightforward, and user-friendly than the grafting-density method.

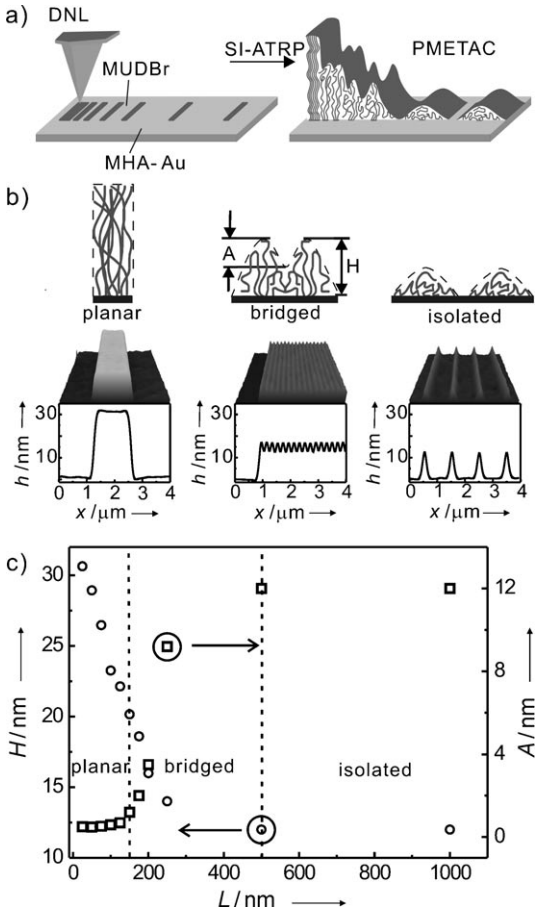

Figure 1. a) 3D polymer structures obtained by control of the spacing between nanobrushes. 1) Linear arrays of MUDBr fabricated by DNL and 2) SI-ATRP of METAC. b) 3D topographic views and average cross-sectional profiles of three typical morphologies of the PMETAC brushes: planar (left), bridged (middle), and isolated (right) with lateral spacings of 25, 200, and 1000 nm, respectively. c) Plots of the height (H; ○) and amplitude (A; □) of the polymer-brush patterns versus the lateral spacing (L).

As proof-of-concept that the spacing of nanobrushes determines morphologies, we first fabricated linear arrays of poly[2-(methacryloyloxy)ethyl-trimethylammonium chloride] (PMETAC) nanobrushes with different lateral spacings by DNL, a scanning probe lithography technique, recently developed by our group, suitable for fabricating nanostructured polymer surfaces.[19] In a typical DNL experiment, an atomic force microscopy (AFM) tip in contact mode was firstly inked with initiator molecules, ω-mercaptoundecyl bromoisobutyrate (MUDBr), and then loaded onto a customized XE-100 atomic force microscope (Park Systems).

[*] Dr. X. Zhou, Dr. X. Wang, Y. Shen, Z. Xie, Prof. Z. J. Zheng
Nanotechnology Center, Institute of Textiles and Clothing
The Hong Kong Polytechnic University, Hong Kong SAR (China)
Fax: (+852) 2773-1432
and
Advanced Research Centre for Fashion and Textiles
The Hong Kong Polytechnic University
Shenzhen Research Institute, Shenzhen (China)
E-mail: tczzheng@inet.polyu.edu.hk

[**] We acknowledge the Hong Kong Polytechnic University (Projects A-PK09, A-PK21, and 1-ZV5Z) for financial support of this project.

Supporting information for this article is available on the WWW under http://dx.doi.org/10.1002/anie.201102518.

The AFM tip was then brought into contact with a gold substrate, of which the surface was previously modified with a self-assembled monolayer (SAM) of 16-mercaptohexadecanoic acid (MHA). Series of linear MUDBr arrays with line-to-line spacings (L) ranging from 25 to 1000 nm were fabricated by shaving the surface with the tip at a contact force of 1000 nN and speed of 1 $\mu m\,s^{-1}$, where the MUDBr initiator displaced the MHA resist at the shaved areas. PMETAC brushes were then grown from the MUDBr templates through a typical surface-initiated atom transfer radical polymerization (SI-ATRP).[19,22–25] The nanobrushes were finally rinsed, dried, and observed by tapping-mode AFM.

Importantly, three typical morphologies of PMETAC nanobrushes, namely isolated, bridged, and planar structures, are observed as function of the line-to-line spacing (L) (Figure 1b). When the nanobrushes are well-separated, for example, at a spacing L of 1000 nm, they form typical isolated linear nanoarrays, in which the maximum height (H), amplitude (A), and lateral width (D) are around 12, 12, and 500 nm, respectively (Figure 1b, right). The width of the nanobrush is much larger than that of the underlying MUDBr template (around 25 nm, see Figure S1 in the Supporting Information). This confinement phenomenon observed at nanoscale has been explained by Jonas et al. using a nanodroplet model that takes into account the surface-wetting energy and the entropy of the polymer chains.[21] Similar to the droplet model, in the present system, the polymer chains can be considered as one-dimensionally confined by the width of the nanobrushes (the length of the linear array is longer than 10 μm and therefore can be considered as infinite). The chains at the edges try to fall and spread laterally on the surface because of the affinity between the quaternary ammonium groups of PMETAC and the carboxylic background of the substrate, which creates extra room for the chains in the center of the linear array to collapse. These overall interactions result in an increase in line width, a decrease in maximum height, and formation of archlike cross-sections (Figure 1b, right). The isolated morphology of the linear nanoarrays remains unchanged until L reaches lateral dimension of 500 nm between the linear nanoarrays.

When the lateral spacing is further decreased from 500 nm to 150 nm, the polymer chains at the peripheral areas of the linear nanoarrays get in contact with those of the neighboring linear nanoarrays and form a bridged structure (Figure 1b, middle). The key characteristic of bridged structure is that H increases while A decreases as a function of decreasing L. When L is less than 500 nm, the PMETAC chains at the edge start to stretch up as a result of steric repulsion of accumulated chains located in neighboring linear nanoarrays. The stretching of the peripheral chains further pushes the polymer chains at the center of the linear nanoarray to stretch up, so that the maximum height increases from 12 to 20 nm (Figure 1c). The difference in stretching rates of chains at the edge and center of linear arrays results in a decreasing amplitude from 12 to 1 nm.

Finally, the morphology enters the planar structure when the lateral spacing is less than 150 nm (Figure 1b, left). At this region, H increases linearly from 20 to 31 nm with a planar top layer ($A < 1$ nm, Figure 1c). The rate of increase in height is around 0.1 nm per nanometer of lateral narrowing, which is much higher than that of the bridged structure. When the spacing reaches 25 nm, which is equal to the footprint of the MUDBr template, we consider all that nanobrushes merge into a two-dimensional sheet equal to that grown from a homogenous SAM of MUDBr on a gold surface. Because all samples were dried by blowing air over the surfaces prior to measurements and the humidity of the laboratory was 40–50% during the experiments, the morphologies were stable during the measurements and even after storage for a few days.

In another set of experiments, PMETAC nanodot arrays (each of $5 \times 5\ \mu m^2$) were also fabricated by DNL with 100 ms indentation at 1000 nN (Figure 2a). A similar morphological

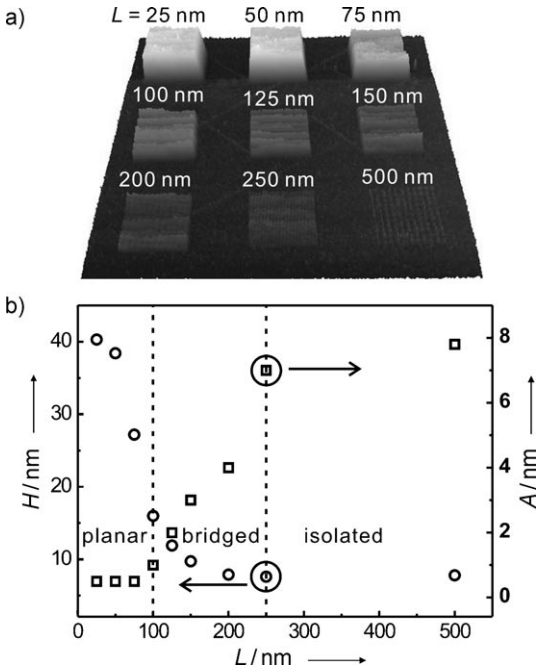

Figure 2. a) 3D AFM topographic image of the 3×3 array of PMETAC-brush patterns with dot–dot spacings of 25, 50, 75, 100, 125, 150, 200, 250, and 500 nm, respectively. b) Plots of the brush height (H; ○) and amplitude (A; □) versus the dot–dot spacing (L).

evolution is observed upon changing of the dot-to-dot spacing between 500 and 25 nm (Figure 2b). The nanobrushes exhibit isolated, dropletlike structures when L is larger than 250 nm. The height and diameter of the isolated nanodots are around 8 and 250 nm, respectively. The structure enters bridged and planar regions when the spacing is below 250 nm, where the height increases from 8 to 41 nm. The height observed during the change from the completely isolated to the completely stretched stage doubles in the case of linear nanoarrays and quadruples for the nanodots. This observation can be explained by the different extend of lateral confinement effects. When the spacing is decreased, each nanodot is in contact with four neighboring nanodots, which will generate stronger lateral confinement effects.

Knowing the relationship between the spacing of nanobrushes to the surface morphology, we can rationally design

and fabricate arrays of nanobrushes with asymmetric spacings which form the desired 3D polymer structures. We first demonstrate how to fabricate polymer gradients, which are important templates to understand the binding behavior in many biological processes.[3,5,8,26] The key step is to generate arrays of nanobrushes with gradual change in their dot-to-dot spacing. This gradual change can be readily achieved by converting a gray-scale gradient image into a density varying black-and-white bitmap with defined pixel number and pixel distance. This bitmap will be used as a guide map for DNL experiments, in which only the black pixels are recognized as "writing" dots. As proof-of-concept, we fabricated gradients of PMETAC brushes with the shape of a simple slide (Figure 3a). A $7.25 \times 1.45\ \mu m^2$ gray-scale gradient along the x direction was first converted into a 146×30 pixels black-and-white bitmap, in which the 100% dark areas of the gray-scale gradient were converted into black pixels that are closely packed, whereas the bright areas were converted into black pixels that are separated by white pixels (Figure 3a inset). Because the height of the nanobrushes significantly changes in the L range from 150 to 50 nm (Figure 2), we define a pixel distance of 50 nm in both x and y directions to obtain a 3D structure with obvious height variations. Finally, DNL was carried out using this guide map, followed by SI-ATRP. The final polymer structure was observed with tapping-mode AFM. Indeed, a $7.55 \times 1.75\ \mu m^2$ slide with a gradual increase in height is observed (see Figure S3 in the Supporting Information). Along the gradient direction, the height of the brushes increases from 0 nm (correspond to the 100% bright areas of the gray-scale gradient) to 35 nm (correspond to the 100% dark areas of the gray-scale gradient), where the height is close to that of the 50 nm spaced dot–dot arrays (Figure 2b). Using the same procedures, we further fabricated symmetric two-dimensional gradients with conic and pyramidal shapes (Figure 3b,c) and asymmetric two-dimensional gradients with a new moon shape (Figure 3d). The nonpatterned areas are free of polymer brushes as shown by AFM (see Figure S4 in the Supporting Information).

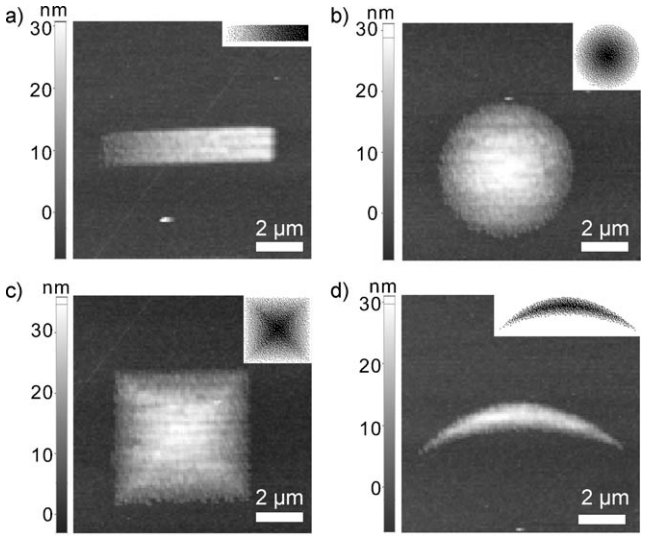

Figure 3. AFM topographic images of the PMETAC-brush gradients with different shapes and their corresponding bitmap images shown in the insets: a) slide, b) cone, c) pyramid, and d) new moon shape.

Most importantly, this simple bitmap-converting method can be extended to fabricate arbitrary 3D polymer structures with complex surface morphologies. We show here the fabrication of a 3D microscale portrait of the Mona Lisa obtained from arrays of PMETAC nanodots. Similarly, a gray-scale image of the Mona Lisa (Figure 4a) was converted into a 175×200 pixel bitmap (Figure 4b) with a distance of 50 nm between the pixels. In the present DNL experiment, the white pixels (12248 in total) were defined as the "writing" pixels. The whole image was patterned in around 40 min at a speed of 200 ms per writing pixel. Figure 4c displayes the image after SI-ATRP from the topological view, in which the height of the polymer brushes is related to the brightness in the grayscale image. Again, the image obtained from the PMETAC brushes is in good agreement with the original image. The height at the most densely packed areas is 35 nm. When this PEMTAC topography is imaged with an optical microscope (Figure 4d), we obtain a portrait of the Mona Lisa very similar to the original gray-scale image, which is a result of the light scattering from the topographic PMETAC structures.

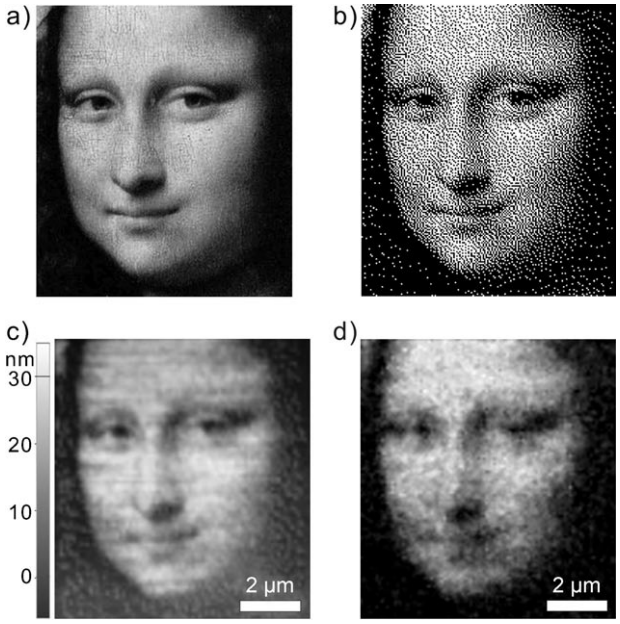

Figure 4. a) Gray-scale and b) bitmap images of the Monalisa. c) AFM topographic image of the Monalisa obtained from PMETAC brushes. d) Dark field image of the Monalisa obtained from PMETAC brushes by reversing a bright field optical microscope image shown in Figure S5 in the Supporting Information.

Our feature-density method is superior in fabrication throughput to the conventional grafting-density method. For example, the number of writing dots required for the portrait of the Mona Lisa ($8.70 \times 9.95\ \mu m^2$) will be 1.38×10^5 pixels by DNL at the smallest feature size of 25 nm. That is, the time needed to finish the patterning by grafting density method will be around 19 days at a writing speed of 200 ms per dot

and therefore around 690-fold longer than the time needed for our feature-density method. Furthermore, the gray-scale converting method is also straightforward and user-friendly and can be readily adapted to any shape and size.

The fabrication principle reported herein can be generally applied for fabricating 3D polymer structures of many different polymers. Apart from the lateral spacing, other parameters such as the degree of polymerization, polymer–substrate interactions, grafting density within each nanobrush, and even environmental factors, such as humidity and temperature, will influence the surface morphology of the polymer brushes. For example, stronger polymer–substrate interactions may lead to stronger wetting of the brushes on the surfaces;[21] the change in grafting densities can affect the height variation of the polymer structures.[13] Therefore, the influence of these parameters should be studied in future experiments.

In conclusion, we have presented a new concept for the fabrication of arbitrary 3D polymer nanostructures, on the basis of defined lateral spacings between assembled nanobrushes. Significantly, this study for the first time reports the discovery that the spacing of nanofeatures directly affects the surface morphology. This will not only lead to a better understanding of confinement effects in polymer nanobrushes, but also provide a platform for systematic investigations on interactions between polymer chains. We believe the present method can be directly applied to create biomimic surfaces for studying cell adhesion, differentiation, and signaling as well as protein interactions. In principle, this strategy can be used with other nanolithographic tools such as e-beam lithography,[20,27,28] nanoimprint lithography,[29,30] nano-shaving/grafting,[31–33] dip-pen nanolithography,[34–36] and polymer pen lithography.[37]

Received: April 12, 2011
Published online: June 9, 2011

Keywords: nanostructures · nanopatterning · polymers · polymerization

[1] M. A. C. Stuart, W. T. S. Huck, J. Genzer, M. Muller, C. Ober, M. Stamm, G. B. Sukhorukov, I. Szleifer, V. V. Tsukruk, M. Urban, F. Winnik, S. Zauscher, I. Luzinov, S. Minko, *Nat. Mater.* **2010**, *9*, 101.
[2] B. D. Gates, Q. B. Xu, M. Stewart, D. Ryan, C. G. Willson, G. M. Whitesides, *Chem. Rev.* **2005**, *105*, 1171.
[3] P. Roach, T. Parker, N. Gadegaard, M. R. Alexander, *Surf. Sci. Rep.* **2010**, *65*, 145.
[4] Z. H. Nie, E. Kumacheva, *Nat. Mater.* **2008**, *7*, 277.
[5] S. Morgenthaler, C. Zink, N. D. Spencer, *Soft Matter* **2008**, *4*, 419.
[6] Y. L. Zhang, Q. D. Chen, H. Xia, H. B. Sun, *Nano Today* **2010**, *5*, 435.
[7] R. Ducker, A. Garcia, J. M. Zhang, T. Chen, S. Zauscher, *Soft Matter* **2008**, *4*, 1774.
[8] R. Ogaki, M. Alexander, P. Kingshott, *Mater. Today* **2010**, *13*, 22.
[9] Y. D. Yan, Z. J. Hu, X. S. Zhao, T. Sun, S. Dong, X. D. Li, *Small* **2010**, *6*, 724.
[10] D. Pires, J. L. Hedrick, A. De Silva, J. Frommer, B. Gotsmann, H. Wolf, M. Despont, U. Duerig, A. W. Knoll, *Science* **2010**, *328*, 732.
[11] A. W. Knoll, D. Pires, O. Coulembier, P. Dubois, J. L. Hedrick, J. Frommer, U. Duerig, *Adv. Mater.* **2010**, *22*, 3361.
[12] R. Barbey, L. Lavanant, D. Paripovic, N. Schuwer, C. Sugnaux, S. Tugulu, H. A. Klok, *Chem. Rev.* **2009**, *109*, 5437.
[13] W. K. Lee, M. Patra, P. Linse, S. Zauscher, *Small* **2007**, *3*, 63.
[14] S. Schilp, N. Ballav, M. Zharnikov, *Angew. Chem.* **2008**, *120*, 6891; *Angew. Chem. Int. Ed.* **2008**, *47*, 6786.
[15] M. Steenackers, R. Jordan, A. Kuller, M. Grunze, *Adv. Mater.* **2009**, *21*, 2921.
[16] M. Steenackers, A. Kueller, N. Ballav, M. Zharnikov, M. Grunze, R. Jordan, *Small* **2007**, *3*, 1764.
[17] N. Ballav, S. Schilp, M. Zharnikov, *Angew. Chem.* **2008**, *120*, 1443; *Angew. Chem. Int. Ed.* **2008**, *47*, 1421.
[18] T. Winkler, N. Ballav, H. Thomas, M. Zharnikov, A. Terfort, *Angew. Chem.* **2008**, *120*, 7348; *Angew. Chem. Int. Ed.* **2008**, *47*, 7238.
[19] X. Q. Liu, Y. Li, Z. J. Zheng, *Nanoscale* **2010**, *2*, 2614.
[20] A. M. Jonas, Z. J. Hu, K. Glinel, W. T. S. Huck, *Nano Lett.* **2008**, *8*, 3819.
[21] A. M. Jonas, Z. J. Hu, K. Glinel, W. T. S. Huck, *Macromolecules* **2008**, *41*, 6859.
[22] S. Edmondson, V. L. Osborne, W. T. S. Huck, *Chem. Soc. Rev.* **2004**, *33*, 14.
[23] F. Zhou, Z. J. Zheng, B. Yu, W. M. Liu, W. T. S. Huck, *J. Am. Chem. Soc.* **2006**, *128*, 16253.
[24] O. Azzaroni, Z. J. Zheng, Z. Q. Yang, W. T. S. Huck, *Langmuir* **2006**, *22*, 6730.
[25] X. Q. Liu, H. X. Chang, Y. Li, W. T. S. Huck, Z. J. Zheng, *ACS Appl. Mater. Interfaces* **2010**, *2*, 529.
[26] C. G. Simon, S. Lin-Gibson, *Adv. Mater.* **2011**, *23*, 369.
[27] S. J. Ahn, M. Kaholek, W. K. Lee, B. LaMattina, T. H. LaBean, S. Zauscher, *Adv. Mater.* **2004**, *16*, 2141.
[28] M. Y. Paik, Y. Y. Xu, A. Rastogi, M. Tanaka, Y. Yi, C. K. Ober, *Nano Lett.* **2010**, *10*, 3873.
[29] S. B. Jhaveri, M. Beinhoff, C. J. Hawker, K. R. Carter, D. Y. Sogah, *ACS Nano* **2008**, *2*, 719.
[30] A. Genua, J. A. Alduncin, J. A. Pomposo, H. Grande, N. Kehagias, V. Reboud, C. Sotomayor, I. Mondragon, D. Mecerreyes, *Nanotechnology* **2007**, *18*, 215301.
[31] S. Xu, G. Y. Liu, *Langmuir* **1997**, *13*, 127.
[32] S. Xu, S. Miller, P. E. Laibinis, G. Y. Liu, *Langmuir* **1999**, *15*, 7244.
[33] M. Barczewski, S. Walheim, T. Heiler, A. Blaszczyk, M. Mayor, T. Schimmel, *Langmuir* **2010**, *26*, 3623.
[34] X. G. Liu, S. W. Guo, C. A. Mirkin, *Angew. Chem.* **2003**, *115*, 4933; *Angew. Chem. Int. Ed.* **2003**, *42*, 4785.
[35] X. Z. Zhou, Y. H. Chen, B. Li, G. Lu, F. Y. C. Boey, J. Ma, H. Zhang, *Small* **2008**, *4*, 1324.
[36] D. S. Ginger, H. Zhang, C. A. Mirkin, *Angew. Chem.* **2004**, *116*, 30; *Angew. Chem. Int. Ed.* **2004**, *43*, 30.
[37] F. W. Huo, Z. J. Zheng, G. F. Zheng, L. R. Giam, H. Zhang, C. A. Mirkin, *Science* **2008**, *321*, 1658.

